



Gaseous and particulate matter (PM) emissions from a turboshaft-engine using different blends of sustainable aviation fuel (SAF)

Marius Rohkamp, Alexander Rabl, Jan Bendl, Carsten Neukirchen, Mohammad Reza Saraji-Bozorgzad, Christian Helcig, Andreas Hupfer & Thomas Adam

To cite this article: Marius Rohkamp, Alexander Rabl, Jan Bendl, Carsten Neukirchen, Mohammad Reza Saraji-Bozorgzad, Christian Helcig, Andreas Hupfer & Thomas Adam (2025) Gaseous and particulate matter (PM) emissions from a turboshaft-engine using different blends of sustainable aviation fuel (SAF), *Aerosol Science and Technology*, 59:1, 111-126, DOI: [10.1080/02786826.2024.2417977](https://doi.org/10.1080/02786826.2024.2417977)

To link to this article: <https://doi.org/10.1080/02786826.2024.2417977>



© 2024 The Author(s). Published with license by Taylor & Francis Group, LLC.



[View supplementary material](#)



Published online: 07 Nov 2024.



[Submit your article to this journal](#)



Article views: 532



[View related articles](#)



[View Crossmark data](#)



Gaseous and particulate matter (PM) emissions from a turboshaft-engine using different blends of sustainable aviation fuel (SAF)

Marius Rohkamp^{a,b} , Alexander Rabl^c, Jan Bendl^a , Carsten Neukirchen^a, Mohammad Reza Saraji-Bozorgzad^a, Christian Helcig^c, Andreas Hupfer^b, and Thomas Adam^a

^aFaculty for Mechanical Engineering, Institute of Chemical and Environmental Engineering, University of the Bundeswehr Munich, Neubiberg, Bavaria, Germany; ^bFaculty for Mechanical Engineering, Institute of Aeronautical Engineering, University of the Bundeswehr Munich, Neubiberg, Bavaria, Germany; ^cTUM School of Engineering and Design, Institute for Turbomachinery and Flight Propulsion, The Technical University of Munich, Garching, Bavaria, Germany

ABSTRACT

Emissions from small gas turbine engines pose environmental and health risks and they are, dependent of engine type and manufacture date, not regulated or only subject to smoke emission standards resulting in a lack of detailed emission characterization. This study examines the emission behavior of an Allison 250-C20B turboshaft engine when powered by different blends (30, 50, and 100%) of Hydroprocessed Esters and Fatty Acids (HEFA) based Sustainable Aviation Fuel (SAF). The change in engine power is linked to differences in gaseous and particulate matter (PM) emissions. Emission indices (EI) for gas phase constituents are reduced at higher power settings due to a higher combustion chamber efficiency resulting from better fuel atomization, fuel-air mixing behavior, and higher flame temperatures. Differences in gaseous EI at the same power setting between the fuels investigated are negligible for all regulated gaseous compounds (UHC, CO, NO_x). However, there are variations in the gaseous volatile organic compounds (VOC) and in polycyclic aromatic hydrocarbons (PAH). Significantly more pronounced changes can be seen in the particulate phase. The non-volatile particulate matter (nvPM) number concentrations were reduced by up to 81% using 100% SAF compared to Jet A-1 fuel. In addition, using SAF shifts the mode of the particle number size distribution (PNSD) to smaller sizes, that is, from the maximum at 55 nm (Jet A-1) to a maximum at 25 nm (100% SAF). This reduces the emitted particle mass up to 76%. The reduction can be explained by the chemical composition of the fuels and the subsequent PAH and soot formation during combustion.

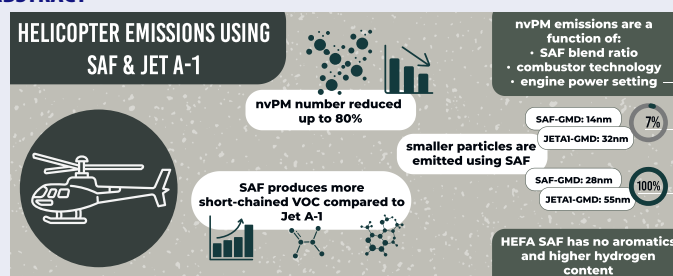
ARTICLE HISTORY

Received 21 May 2024
Accepted 9 October 2024

EDITOR

Jason Olfert

GRAPHICAL ABSTRACT



Introduction

Sustainable aviation fuels (SAF) are increasingly being implemented in global civil and military flight operations. The advantage of SAF is the drop-in technology: it can be used without modifying the airport

infrastructure or adapting the engine technology. SAF are not produced from crude oil like regular Jet A-1 kerosene but are biogenic or synthetic. SAF can be divided into different categories including biofuels produced from biogenic waste and synthetic or

CONTACT Marius Rohkamp m.rohkamp@unibw.de University of the Bundeswehr Munich, Faculty for Mechanical Engineering, Werner-Heisenberg-Weg 39, 85577 Neubiberg, Germany.

Supplemental data for this article can be accessed online at <https://doi.org/10.1080/02786826.2024.2417977>.

© 2024 The Author(s). Published with license by Taylor & Francis Group, LLC.

This is an Open Access article distributed under the terms of the Creative Commons Attribution-NonCommercial-NoDerivatives License (<http://creativecommons.org/licenses/by-nc-nd/4.0/>), which permits non-commercial re-use, distribution, and reproduction in any medium, provided the original work is properly cited, and is not altered, transformed, or built upon in any way. The terms on which this article has been published allow the posting of the Accepted Manuscript in a repository by the author(s) or with their consent.

synfuels produced through power-to-liquid (PtL) technologies. Both fuels are low in aromatic hydrocarbon compounds including naphthalene and contain almost no sulfur (Owen et al. 2022).

The sustainable production chain is therefore not the only positive aspect of SAF. They have been reported as reducing non-CO₂ emissions, for example, soot particles (Durdina et al. 2021; Corbin et al. 2022), thus improving the air quality around airports, and decreasing the impact on climate change. The use of SAF, therefore, plays a major role in achieving carbon dioxide (CO₂) neutrality in aviation by 2050. SAF is associated with “sustainable flying”, although climate-damaging exhaust gases are nevertheless produced through its use. Another aspect in the context of global warming is that the reduction in number of soot particles can result in a reduction in contrail formation and subsequently in less radiative heating (Lee et al. 2021). However, the final effect of contrails, negative or positive, has not yet been clarified. Fundamental research in this area is being carried out to analyze the effects of burnt SAF to reduce the global warming impact of airline contrails (Voigt et al. 2021). To better understand the complex formation mechanisms of PM and the resulting contrails with their (radiative forcing) effects, engine ground tests are important as they provide the basis for understanding the chemical and physical properties of the emissions.

In general, the chemical composition of gas turbine emissions depend on type and design of the engine and on the fuel used. Emission formation begins inside the combustion chamber. In the first step the liquid fuel is atomized, vaporized and thoroughly mixed with the compressed air (step 1: injection and mixing). The fuel-air mixture must have a sufficient residence time at high temperatures (Lieuwen and Yang 2013), which can be influenced by the combustion chamber design, for example, with cooling air holes (step 2: combustion). With different designs, which all must fulfill requirements, the specific emission characteristics of the combustion chamber, and thus the engine, changes.

For step 1 modern engines use air-assisted atomization or vaporizer allowing a better fuel-air mixture with less fuel-rich combustion zones and lower nitrogen oxides (NO_x) emissions compared to standard pressure spray atomizer (Hupfer 2007; Lefebvre and Ballal 2010). After injection, the combustion chamber design determines step 2 and the following emission formation. Rich-Burn Quick-Quench Lean-Burn (RQL), Lean-Direct-Injection (LDI) or Lean-

Premixed-Prevaporized (LPP) are examples of concepts for low-emission combustion chamber technologies. Different equivalence ratios are established in the combustion chamber depending on the engine power setting. Non-volatile PM (nvPM) or soot formation occurs mainly in the primary zone close to the fuel spray, where fuel and air are not well mixed. By additional dilution, carbon monoxide (CO) and soot can be post-oxidized. Peak concentrations of NO_x can occur due to the high temperatures in the combustion chamber (Owen et al. 2022). RQL combustion chambers are known to increase PM and CO formation because of the rich combustion in their primary zones (Harper et al. 2022; Owen et al. 2022). LDI and LPP combustors have, due to their leaner fuel-air ratio (FAR), which is below the stoichiometric ratio, lower NO_x and PM emissions but have other drawbacks, for example, reduced flame stability due to the lean combustion zone (Hupfer 2007). These technologies rely on the fact that the production of NO_x significantly rises with temperature, therefore aiming to minimize stoichiometric combustion zones whenever feasible (Hicks and Tacina 2021).

Smaller and less modern engines, like the Allison 250-C20B used in this study, contain a pressure atomization nozzle, which produces locally fuel-rich combustion zones depending on the engine power setting. Compared to large and modern gas turbine engines, fuel and air are not well mixed resulting in high emissions of unburned hydrocarbons (UHC) and soot. However, a key advantage is that this design exhibits a very robust approach for testing different fuels.

In summary, it can be said that injection and mixing differ due to different combustor technologies. Gas turbine emission behavior strongly depends on the engine power settings as they influence local thermodynamic states/properties and chemical reaction processes. The goal of low emissions, efficient combustion and homogeneous temperature distribution inside the turbine is related to the atomization and fuel-air mixing in the combustor.

The International Civil Aviation Organization (ICAO) regulates gaseous emissions (UHC, CO, and NO_x) and smoke respectively non-volatile PM mass and number (ICAO 2023). When applying the emission limits, a distinction is made between turbojet and turbofan engines with rated thrust of less and more than 26.7 kN and the date of manufacture. For example, turbojet and turbofan engines below 26.7 kN are only regulated for smoke. In general, emissions from turboshaft engines are not included in the regulations of ICAO Annex 16 Volume II.

While there is the ICAO Aircraft Engine Emissions Databank for turbojet and turbofan engines, there is a lack of reference data for small turbofan (lower 26.7 kN thrust), turboprop and turboshaft engines. As the emissions of these engines are not regulated, it is necessary to characterize them and expand the available data.

Several studies reported the influence of SAF on the emission behavior of turbofan engines (Boies et al. 2015; Moore et al. 2015; Durdina et al. 2021; Corbin et al. 2022; Durdina et al. 2024) or turboshaft engines (Drozd et al. 2012; Cain et al. 2013; Kinsey et al. 2019). Previous studies (Brem et al. 2015; Durand et al. 2021; Harper et al. 2022) link the fuels' hydrogen content to the nvPM emissions. A relation was also shown between the total volatile PM mass and number, the sulfur (Wey et al. 2006), and the naphthalene (Schripp et al. 2022) content. Other studies, for example, the alternative aviation fuel experiment (AAFEX), found out that independent of the power setting of the engine EI for nvPM number increase linearly with the aromatic content and decrease with the hydrogen content of the fuel (Anderson et al. 2011; Brem et al. 2015; Moore et al. 2015). Studies, which used a comparable helicopter engine and SAF, showed that paraffinic fuels produce significantly lower PM number and mass emissions relative to aromatic-containing fuels (Cain et al. 2013).

To our knowledge, the influence of SAF and their blends with Jet A-1 on emission formation, in particular, their influence on PAH and soot formation of turboshaft engines for helicopters and the resulting possible improvement of local air quality has not been thoroughly investigated yet, which is subject of the here presented research.

Experimental methodology

Sampling system and instrumentation

Gaseous and PM emissions were detected directly at exhaust exit of the engine (see Figure 1). Two probes were utilized – a single-hole probe for the gas phase (5 mm inner diameter (i.d.)) and a multi-orifice probe for the aerosol (9 mm i.d., with 16 sampling orifices with an equal hole diameter of 6 mm). The PM probe was placed upstream of the gas sampling probe to keep losses which could arise from turbulences and flow instabilities as low as possible. This was also intended to avoid a possible recirculation area, which could produce measurement artifacts. The focus of the study was on nvPM with diameters up to 200 nm. PM

losses that arise from sampling are explained in more detail in “PM losses” section.

The gaseous emissions were transferred with a 5 m heated transfer line and an i.d. of 4 mm (Winkler GmbH, Heidelberg, Germany), which was kept to a constant temperature of 200 ± 5 °C. As first, the gaseous emissions were analyzed with a Fourier-Transform-Infrared (FTIR) spectrometer system (DX4000, Gaset, Karlsruhe, Germany). The system determines the main gaseous components as wet concentrations, so no correction from dry or semi-dry to wet conditions had to be made. The FTIR does not meet ICAO specifications (ICAO 2023) for measuring CO₂, CO, and NO_x, but it was still used as the FTIR can measure the regulated and additional components at the same time. The oxygen (O₂) content was measured with an O₂-Analyzer (PM 10, M&C TechGroup, Ratingen, Germany) and UHC were analyzed with a flame-ionization-detector (FID), both connected to the outlet of the FTIR. The FID (Thermo-FID, SK-Elektronik, Leverkusen, Germany) specifies the UHC in the exhaust in an equivalent of C₃H₈ (propane). Before each testing day it was calibrated with a 30 ppm propane calibration gas (Linde GmbH, Pullach, Germany). In addition, a gas chromatograph (GC) with two FID-detectors was connected behind the FTIR to measure the content of volatile organic compounds (VOC), referred to as VOC-GC (8890, Agilent Inc., Santa Clara, CA). Focus in this study was on C₂–C₉ hydrocarbons, which are listed as ozone precursors for ambient air in the European Union (EU Directive 2008). A detailed description on the system and the analytical approach including the calculation of ozone formation potentials can be found in Rohkamp et al. (2024) and Adam et al. (2011) and references therein. The VOC-GC was connected to the outlet of the FTIR by a 9 m PTFE tube (5 mm i.d.) and located outside the engine test cell to avoid overheating. Total flows of the gas phase measurements were 3.5 l/min for FTIR, 0.3 l/min for FID, 0.5 l/min for O₂ and 0.3 l/min for GC analysis. Before each sampling for GC-analysis, the line was purged for 5 min to remove any residual emissions from previous engine power settings. However, during testing stable measurement values for the respective operating points were reached after approx. 30 s.

PM emissions were guided *via* a heated transfer line of 10 mm i.d. (H3450, Hillesheim GmbH, Waghäusel, Germany) kept to 200 ± 5 °C. Before entering the two-stage dilution system (eDiluter Pro, Dekati, Kangasala, Finland) a cyclone with a cutoff point of 2.5 μm was implemented to protect the

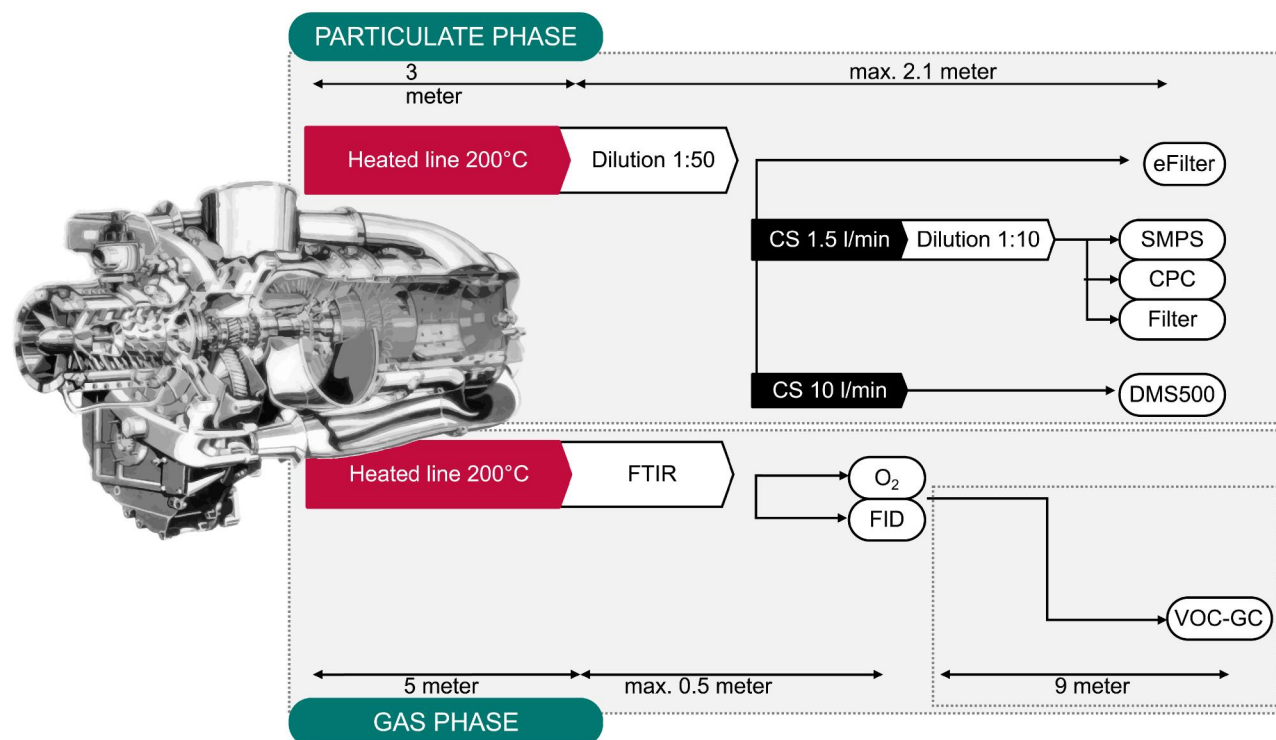


Figure 1. Experimental setup.

downstream connected systems from potential clogging by particle clusters. Clean air supply was provided by a compressor (SF2FF, Atlas Copo, Essen, Germany), a tank (500 liter with max. 11 bar, OKS Otto Klein GmbH, Kreuztal, Germany), and a zero-air generator (737-Series, Aadco Instruments, Inc., USA), which generated particle and VOC free air. Prior to the first dilution stage, compressed air was heated to 200°C to mainly reduce thermophoretic losses. The purity of the dilution air and the tightness of the sampling lines and instruments were tested prior each measurement day. After the dilution, two outlets were used to connect the devices. At one outlet, the Differential Mobility Spectrometer (DMS500, Cambustion, Cambridge, United Kingdom) and the setup for the gravimetric PM filter sampling (eFilter, Dekati, Kangasala, Finland) were connected. The DMS500 determines the particle size distribution (PSD) and measures the particle mobility diameter. To ensure that only non-volatile soot particles were measured, a catalytic stripper (CS, CS10, Catalytic Instruments, Rosenheim, Germany) was placed upstream of the DMS500. At the second line, a smaller-sized CS (CS015, Catalytic Instruments, Rosenheim, Germany) and an additional dilution stage (VKL 10 with 2-5 l/min isokinetic suction nozzle, Palas, Karlsruhe, Germany) were connected to ensure that the Condensation Particle Counter (CPC) was operated in single counting mode. Furthermore, a

Scanning Mobility Particle Sizer (SMPS, 5420 with M-DMA, Grimm, Ainring, Germany) and a CPC (5420 without DMA, Grimm, Ainring, Germany) were attached for further measurements. The SMPS measures PSD and mobility diameter, like the DMS500, but the DMS500 classifies aerosols much faster. The SMPS is using a CPC for quantification, while the DMS500 utilizes electrometer amplifiers for charged particle detection. In addition, the instruments also differ in the charging method of aerosols. While the SMPS charges the particles bipolar for precise size measurements, the unipolar charging of the DMS500 enables fast, real-time measurements, leading to potential concentrations uncertainties between both systems. DMS500 was calibrated for spherical aerosols and not for soot. This results in higher number concentrations when measuring nvPM with DMS500.

Additionally, a pump (BiVOC2V2, Holbach, Wadern, Germany) was attached to achieve the required volumetric flow rates for the VKL 10 nozzle. The nozzle needed at least 2.0 l/min for isokinetic dilution with the SMPS and CPC consumed each 0.3 l/min. The 47 mm polycarbonate filters for gravimetry were weighed prior and after sampling at least five times using a micro-balance (Cubis II MCA2.7S-2S00-F, Sartorius, Göttingen, Germany). The filters were conditioned (temperature: 22°C, air density: 1.117 kg/m³, relative humidity: 45%, filter charge neutralizer) in a weighing chamber (pureGMC18, pure

engineering, Weinstadt, Germany) for at least 24 hours before and after sampling. To check the stability of the chamber, a reference filter was weighed for each weighing process. Moreover, filter samples were collected for later offline analyses, for example, scanning electron microscopy (SEM).

Turboshaft-engine details and measurement cycle

The Allison 250-C20B, also known as Allison T63, is a turboshaft engine designed and produced by Rolls-Royce Corporation (formerly Allison Engine Company) and is known for its reliability and widespread use in various applications, especially in the aerospace helicopter industry. The compressor consists of six axial and one radial compressor stage leading the pressurized air into the single can-type combustion chamber. The primary air component for combustion is about 25% of the total air, the remaining secondary air is used for cooling. The fuel is injected by one nozzle, which is a single-entry dual orifice pressure swirl atomizer. It is a duplex style fuel nozzle with two flow patterns with a spring inside, which changes the flow pattern when the fuel pressure is high enough. The low fuel injection pressure at low engine power results in a local fuel-rich and fast-quenched flame producing comparatively high UHC and CO emissions. More fuel is injected into the combustion chamber under higher pressure at higher power settings. The engine and also the combustor were designed for this operating point. Due to the better mixing, significantly lower emissions for UHC and CO are reached, as the local conditions for faster chemical reactions are improved. However, this does not apply to NO_x and PM as the conditions for their formation are favorable higher pressures and temperatures. A detailed description of the combustion chamber and the individual components can be found in Klingshirm et al. (2012). Further details on how the combustion chamber design influences the emissions will be provided in the data evaluation in “Gaseous emissions” section and “Non-volatile particulate matter emissions” section.

After leaving the combustion chamber, the hot exhaust gases pass through the two-stage gas generator turbine, followed by a two-stage power turbine. The power from the power turbine shaft is passed through the gearbox to reduce its rotational speed before being transmitted to the output shaft. An Eddy-Current-Brake was used to determine and measure the engines delivered torque load. An overview of

several physical parameters of the gas turbine at the engine power settings Ground Idle (GI) and Take-Off (TO) are listed in Table 1.

The engine power settings were applied based on the ICAO Landing-Take-Off (LTO) cycle (ICAO 2023), which consists of four thrust settings (100, 85, 30, and 7% of rated thrust) for representative flight phases (take-off, climb, approach and ground-idle or taxi). As the LTO cycle does not apply to turboshaft engines, the terms medium-load (ML) and low-load (LL) are used instead of climb and approach.

Fuel properties

Table 2 lists the properties of the tested fuels. The standard requirements for aviation turbine fuels set by the American Society for Testing and Materials (ASTM) are listed first. This is followed by the properties of the reference Jet A-1 (Ref Jet A-1) and then of the SAF used, in this study a fuel from hydroprocessed esters and fatty acids (HEFA). Fuel properties (C/H contents) were determined with ASTM D5291. The hydrogen to carbon (H/C) ratio, also defined as α , is needed for calculation of gaseous EI and can be determined with the molar masses of the respective species. Ref Jet A-1 was used as an admixture with proportions of 70% for the HEFA 30% blend (declared as 30% SAF) and 50% for the HEFA 50% blend (declared as 50% SAF) and is used as a comparison to the blends and pure SAF.

Measurement procedures and analysis

The engine test runs always followed the same procedure. First, the engine was warmed up in GI. This was followed by TO, ML, LL, and GI engine power settings. For the interpretation of GI emissions, only GI runs after warm-ups were taken into account.

All measurement data sets were reduced to the respective times of the engines power setting and averaged. For gaseous emissions, a stable UHC value was awaited for to assume that the respective power setting was stable, as the FID exhibits the most inertial asymptotic behavior. Regarding nvPM, the measurement duration was adapted to the SMPS, as this required approximately 3 min for a scan from 5 to 350 nm. For this reason, at least three scans were carried out before the next power setting was selected. The PM mass was determined using gravimetric filter sampling. Sampling was terminated shortly before the engine power setting was changed. On average, each

Table 1. Parameters of the turboshaft engine for the power settings GI and to.

	7% rated power – Ground-Idle	100% rated power – Take-Off
Fuel pressure [bar]	13	27
Fuel flow [g/s]	7.5	24
Total temperature combustor outlet [K]	907	1212
Total temperature combustor inlet [K]	399	536
Shaft power [kW]	17.5	250

Table 2. Properties of the fuels used.

	Hydrogen [weight %]	C/H ratio [mass-weighted]	H/C ratio [mol-weighted] α	Total Aromatics [vol.%]	Total Sulfur [weight %]	Napthalene [vol%]	Density at 15 °C	Net heat [MJ/kg]	Smoke point [mm]
ASTM Specification	–	–	–	max. 26.5	max. 0.30	max. 3.0	775 to 840	min. 42.8	min. 18.0
Ref Jet A-1	14.01	6.14	1.94	15.8	0.09	0.8	799.3	43.1	24.3
30% SAF	14.36	5.97	1.99	11.1	0.06	0.6	791.1	43.3	29.7
50% SAF	14.57	5.86	2.00	7.9	0.04	0.4	785.5	43.5	34.3
100% SAF	15.10	5.62	2.12	<0.2	<0.0001	0.0	771.8	44.0	>45.0

filter was exposed to the already diluted (1:50) aerosol for 12 min during the setting of the turboshaft engine.

The averaged data sets of the respective test runs were then compared, and the relative standard deviations were calculated. In addition, care was taken to ensure that the tests were conducted over several days to consider variations in environmental conditions such as temperature, air pressure and humidity. All measured values were corrected to standard temperature and pressure (STP) conditions if this was not already done automatically by the analyzers themselves.

Emission index calculation

There are different approaches for calculating EI for gaseous compounds as well as PM number and mass. The outcome of every approach is a specific EI reported as mass of emission per mass of burnt fuel in [g/kg], [# /kg], and [mg/kg], respectively. On the one hand, gaseous EI can be calculated based on the matrix solution of the chemical combustion equation following ICAO Annex 16 Vol. II (ICAO 2023) and SAE ARP 1533 C (SAE 2016). On the other hand, there are different calculation approaches (e.g., Wey et al. 2006 or Rindlisbacher and Chabbey 2015), which provide fast but power-dependent results. A comparison with deviations of the alternative gaseous EI calculation methods is provided in S1 of the [Supporting Information](#). A fundamental difference between the methods is the assumption of complete combustion (UHC, CO, NO_x are negligible compared to CO₂) and the consideration of the fuel composition. Since comparatively high UHC is emitted at low engine power settings, the EI for UHC, CO, and NO_x of the regulated gaseous emissions were determined using the ICAO method (ICAO 2023). EI for VOC-GC measurements were calculated with the “APEX-Method 2”

and the adjusted pre-factor (see Section S1 of the [Supporting Information](#)).

In addition, there are different approaches for calculating EI of PM mass and number, which, however, are also based on the measured CO₂ value and calculated EI_{CO2}. Based on Moore et al. (2017) and SAE ARP 6481 (SAE 2019), the EI for number (EI_{numberEP10}) and mass (EI_{massEP10}) were calculated as follows:

$$EI_{numEP10} = \frac{nvPM_{num} \cdot k_{SLnum} \cdot S(X)}{\Delta CO_2} \cdot EI_{CO_2} \quad (1)$$

$$EI_{massEP10} = \frac{nvPM_{mass} \cdot k_{SLmass} \cdot S(X)}{\Delta CO_2} \cdot EI_{CO_2} \quad (2)$$

where $nvPM_{num}$, $nvPM_{mass}$ and ΔCO_2 are the dilution-corrected and background-corrected peak areas of the measured nvPM and CO₂ at STP. The CO₂ value was taken from the FTIR while the dilution-corrected PM number and mass were used from CPC and SMPS. EI_{CO2} was calculated according to ICAO Annex 16 Vol. II and was adapted to the fuel properties, as the hydrogen content and thus the maximum CO₂ emissions decrease. The factors k_{SLnum} and k_{SLmass} correct for system and thermophoretic losses, to estimate the nvPM number and mass concentrations at the engine exhaust nozzle exit plane (EENEP) (SAE 2019). Further details can be found in the following section “PM losses”. In addition, a unit-conversion factor $S(X)$ is needed (particle concentrations: number or mass per air volume at STP and gas concentrations: ppm by volume) (Moore et al. 2017):

$$S(X) = \begin{cases} V_m/M_{CO_2} & \text{for particles} \\ M_x/M_{CO_2} & \text{for trace – gases} \end{cases} \quad (3)$$

The result of the calculation is an EI, which is referred to as EI_{numEP10} respectively EI_{massEP10} and indicates that only engine exhaust exit plane particles with diameters between 10 and 1000 nm are used to

determine the nvPM number and mass system loss correction factors (SAE 2019). Further explanations and the derivation of the PM EI can be found in S2 of the [Supporting Information](#).

PM losses

PM losses for aircraft emission measurements can be mainly caused by three issues: sampling, transport in tubes and losses in instrumentation. In detail, the main losses of aircraft nvPM are diffusional, thermophoretic, inertial, electrostatic and bend losses (Durand et al. 2023). The nvPM sampling and measurement system described in the SAE standard ARP6320 has significant size-dependent losses ranging up to around 50% for nvPM mass and up to approximately 90% for nvPM number concentration (SAE 2019). Losses vary based on particle size and are influenced by engine power setting, combustor technology, and other factors (SAE 2019). System losses and their uncertainties increase with decreasing particle size. Correction-methodologies for calculating the system losses are discussed, for example, in SAE AIR6504 (SAE 2022) or by Durand et al. (2023).

In this study, effects, for example, due to non-isokinetic sampling, were not corrected by calculation. However, care was taken during setup to use short, constantly heated lines and to dilute the aerosol as fast as possible. Isokinetic sampling was omitted throughout the measurements, as Brownian motion overwhelms any potential effects of flow velocity variation. The inherent randomness of particle movement driven by Brownian motion supersedes the need for isokinetic sampling in accurately assessing particles smaller than 1000 nm (Kulkarni, Baron, and Willeke 2011; Hinds and Zhu 2022). The online analyzers could not detect particles larger than 1 μm . Due to the cyclone used with a cutoff point of 2.5 μm , this PM diameter could be detected in the offline analysis (e.g., SEM). No particles larger than 200 nm could be detected by previous measurements (Rohkamp et al. 2024), accordingly, this was set as the upper limit of the measured aerodynamic diameter.

Sampling and system losses were calculated using SAE ARP 6481 (SAE 2019). The calculation tool included with the standard calculates the correction factors k_{SLnum} and k_{SLmass} . Using these correction factors, the measured nvPM_{num} and $\text{nvPM}_{\text{mass}}$ concentrations can be related back to the EENEP. The factors include thermophoretic losses of the CS and from the sampling probe to the diluter, losses due to sampling lines (bending and flows) and a CPC efficiency correction.

Thermophoretic losses from the sampling probe to the diluter were calculated as follows in accordance with ICAO/SAE specifications:

$$k_{\text{thermo}} = \left(\frac{T_1 + 273.15}{T_{\text{EGT}} + 273.15} \right)^{-0.38} \quad (4)$$

The exhaust exit gas temperature T_{EGT} was measured direct at the engine exhaust exit with a thermocouple type K (GI: 765 K, LL: 785 K, ML: 855 K, TO: 868 K). The sample tube temperature T_1 was set and controlled with the heated transfer line (473.5 K). As a result, the correction factor k_{thermo} ranged from 1.20 to 1.26 between GI and TO and was applied to the calculation. Thermophoretic losses of the eDiluter were neglected. In addition, the SMPS size distributions were corrected with the vendors' software for multiple charge, DMA and CPC efficiency ($D_{50} = 4.58 \text{ nm}$ and $D_{90} = 10.60 \text{ nm}$).

The relevant literature (Kulkarni, Baron, and Willeke 2011; SAE 2019, SAE 2022; Hinds and Zhu 2022; Durand et al. 2023) should be used to carefully consider sampling losses. However, the size-dependent losses must be taken into account especially when comparing number concentrations to avoid an overestimation of particle reductions due to the formation of smaller particles. More details on the calculation of losses in this study can be found in S3 of the [Supporting Information](#).

Results and discussion

Gaseous emissions

At first, the general combustion products (referred as standard gaseous compounds) analyzed with the FTIR/FID/ O_2 -system are discussed. Afterwards, the gaseous C_2 - C_9 VOC results, measured with the VOC-GC and other relevant exhaust constituents are presented.

Standard gaseous compounds

Figures 2a–e show the averaged EI for UHC, CO, and NO_x . Figure 2a illustrates the power-setting-dependent change in the gas phase for Ref Jet A-1, which was used for blending. Figures 2b–e visualize the differences in the respective power setting for the fuels used. As indicated in “Introduction” section, at higher engine power settings (e.g., TO and ML), the resulting FAR is more homogeneous with less fuel-rich zones, thus the conversion of the fuel is more efficient leading to lower EI for UHC and CO. For TO EI_{UHC} ranges between 0.61 and 0.70 g/kg and EI_{CO} ranges from 13.49 to 15.29 g/kg for all fuels. At GI, EI_{UHC}

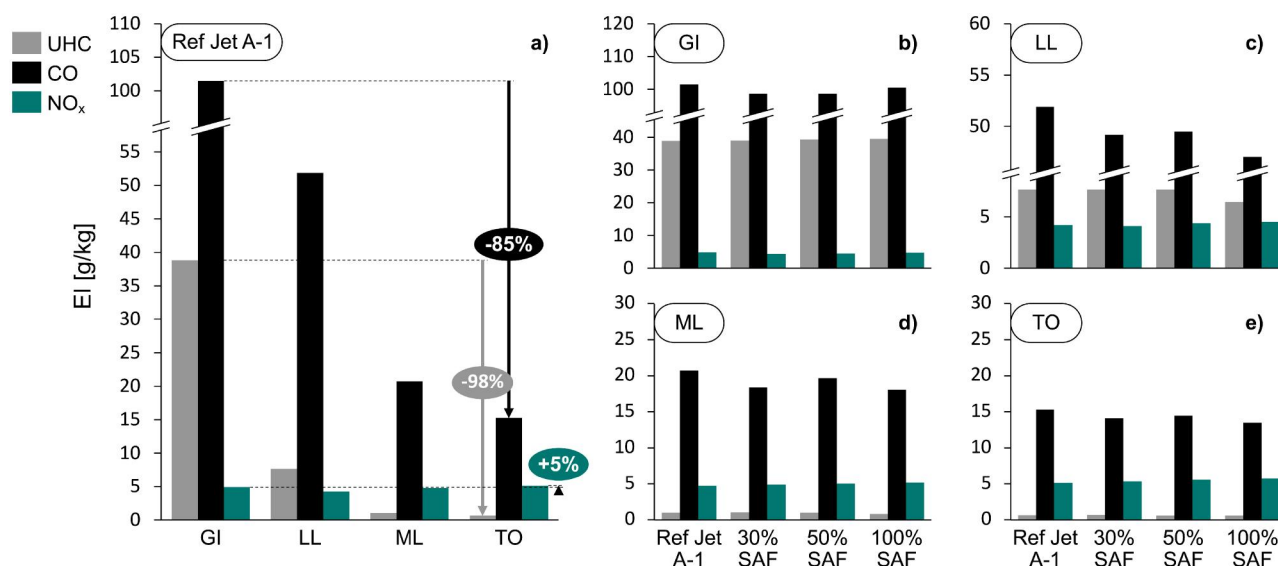


Figure 2. EI [g/kg] for UHC, CO and NO_x calculated with the ICAO/SAE-Method.

risers between 38.85 to 39.56 g/kg and 98.62 to 101.48 g/kg for EI_{CO}. High EI_{UHC} and EI_{CO} represent an inefficient FAR in the combustion chamber with not sufficient O₂ in the primary zone. Since the injected amount of fuel is low, the exhaust gas is cooled very quickly, and the chemical reactions are slowed down or even stopped. The insufficiently high temperatures in the combustion chamber, which are due to the low pressure ratio in the compressor, lead to minimal changes in EI_{NO_x} under different power settings and fuels. EI_{NO_x} ranges from 5.74 to 4.40 g/kg for all fuels and increases up to almost 5% for Ref Jet A-1, see Figure 2a. The corresponding standard deviations were not shown graphically as they are negligible (largest deviation for EI_{CO} at GI power setting with 101.5 ± 3.3 g/kg for Ref Jet A-1).

During other studies (e.g., APEX) it was observed that at engine power settings higher than 15% (comparable to LL) of rated power, engine combustion efficiency was close to 100% resulting in UHC emissions often below the detection level (Masiol and Harrison 2014). Similar behavior can be seen in Figure 2a, where UHCs are reduced by 98% and CO by 85% from GI to TO.

In summary, it can be said that EI of the standard gaseous compounds only change significantly due to the engine power setting, but not because of the fuels used. This supports the declaration that SAF are described as “drop-in” fuels.

Volatile organic compounds

Tables 3 and 4 list the EI of the VOC-GC measurements. Both tables list the total UHC value (measured with the FID as propane and converted to a methane-

Table 3. VOC EI [g/kg] for Ground-Idle engine power setting.

Compound		Ref Jet A-1	30% SAF	50% SAF	100% SAF
UHC (FID)	CH ₄	38.851	39.037	39.371	39.562
Acetylene	C ₂ H ₂	0.5*	0.4*	0.4*	0.4*
Ethylene	C ₂ H ₄	4.4*	4.8*	5.2*	5.6*
Ethane	C ₂ H ₆	0.229	0.250	0.265	0.290
Propylene	C ₃ H ₆	2.752	3.384	3.777	4.393
Butadiene	C ₄ H ₆	0.216	0.731	0.343	0.667
cis-Butene	C ₄ H ₈	0.134	0.166	0.189	0.214
trans-butene	C ₄ H ₈	0.837	1.103	1.109	0.912
1-Pentene	C ₅ H ₁₀	0.516	0.364	0.399	0.358
Benzene	C ₆ H ₆	0.579	0.463	0.338	0.263
Toluene	C ₇ H ₈	0.311	0.283	0.234	0.210
m-xylene	C ₈ H ₁₀	0.253	0.183	0.125	n.a.
1,2,4-Trimethylbenzene	C ₉ H ₁₂	0.387	0.275	0.161	n.a.

equivalent) first, followed by the C₂–C₉ compounds included in the total UHC value (measured with the VOC-GC).

It is noticeable that significantly higher concentrations of ozone precursors are present at the GI power setting, which results from the physical combustion effects already discussed. In addition, only hydrocarbons greater than 0.1 g/kg are shown in Table 3. In principle, EI for ethylene (C₂H₄), propylene (C₃H₆), trans-butene (C₄H₈), butadiene (C₄H₆), benzene (C₆H₆), and acetylene (C₂H₂) have the highest concentrations for all fuels (see Figure 3). In Table 3 EI for C₂H₂ and C₂H₄ are marked with * due to the manual calculation of the concentration. All EI under 0.4 g/kg were summarized in “Others”. With 100% SAF, it is noticeable that the short-chained hydrocarbons (C₂–C₄) have higher EI than with the blends with 30% and 50% (e.g., propylene: 4.39 g/kg for 100% SAF and 3.38 g/kg for the 30% blend and 2.75 g/kg for Ref Jet A-1). The same applies to the long-chained hydrocarbons, but here the opposite behavior occurs – the blends

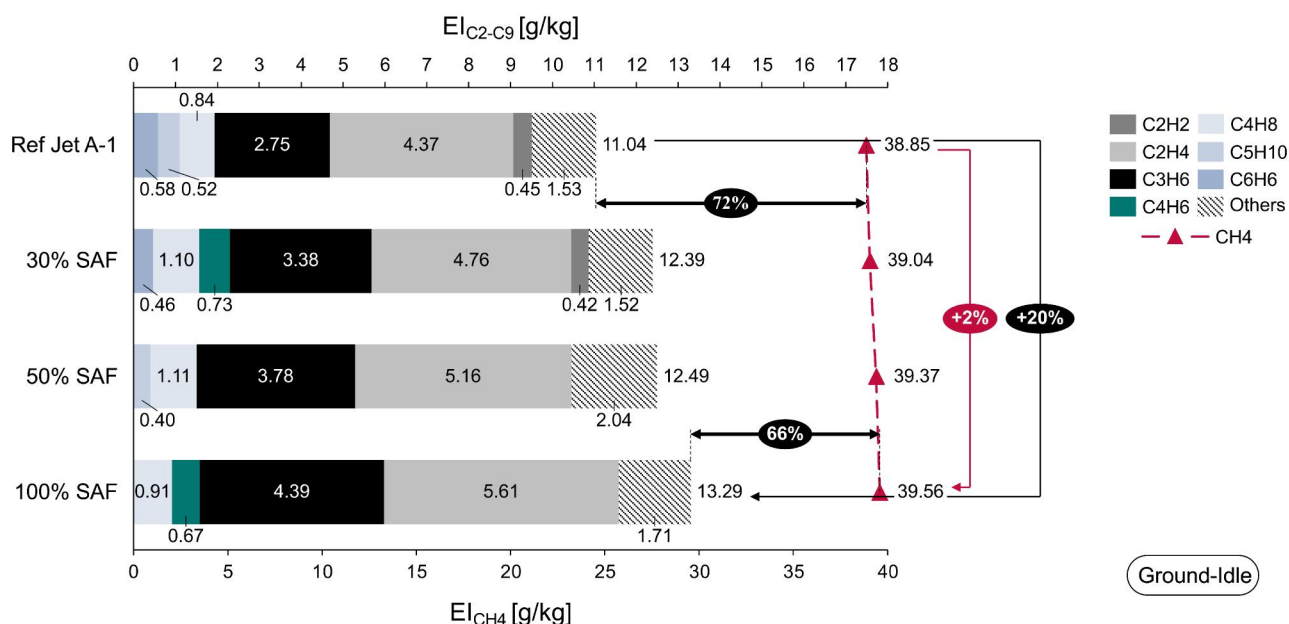


Figure 3. EI for methane (CH_4) and the ozone precursors $\text{C}_2\text{--C}_9$ for the engine power setting GI.

Table 4. VOC EI [g/kg] for Take-Off engine power setting.

Compound		Ref Jet A-1	30% SAF	50% SAF	100% SAF
UHC (FID)	CH_4	0.662	0.703	0.636	0.615
Acetylene	C_2H_2	0.065	0.055	0.052	0.041
Ethylene	C_2H_4	0.140	0.133	0.145	0.132
Propylene	C_3H_6	0.044	0.045	0.050	0.047
Benzene	C_6H_6	0.030	0.024	0.018	0.011
1,2,4-Trimethylbenzene	C_9H_{12}	n.a.	0.020	n.a.	n.a.

feature higher mass concentrations than pure SAF (e.g., benzene: 0.263 g/kg for 100% SAF and 0.463 g/kg for the 30% blend). In case of Ref Jet A-1 fuel, the emissions contain more long-chained hydrocarbons compared to SAF fuels (e.g., 1,2,4-trimethylbenzene: 0.387 g/kg for Ref Jet A-1 compared to 0.161 g/kg for the 50% blend). For GI, Figure 3 illustrates that VOC can increase by 20% when SAF is used, while in turn, the total sum of hydrocarbons measured with the FID remains almost constant (2% deviation).

It is obvious in ground-level operations at airports that high yields of ozone precursors are emitted and might have a major impact on local air quality.

In contrast, the concentrations of all analyzed compounds are significantly reduced during TO engine power, sometimes even below detection limit of the VOC-GC. Therefore, in Table 4 only hydrocarbons with EI higher than 0.01 g/kg are listed. In contrast to GI, the use of SAF at higher engine power can lead to a reduction (see Figure 4) in total ozone precursor concentration. All EI below 0.02 g/kg were summarized in “Others”. A comparison of Jet A-1 with 30% blend shows that there are almost no changes in

concentrations of the VOC. With 50% SAF as well as with 100% SAF content, a reduction in VOC is more evident at TO engine power setting.

$\text{EI}_{\text{CH}_2\text{O}}$ (formaldehyde) and $\text{EI}_{\text{C}_2\text{H}_4\text{O}}$ (acetaldehyde), measured with the FTIR and processed with “APEX Method 2” (Section S1 of the Supporting Information), seem to increase with the addition of SAF. This can be seen in the engine power setting GI – where $\text{EI}_{\text{CH}_2\text{O}}$ increases from 3.24 g/kg with Ref Jet A-1 to 4.13 g/kg with 100% SAF (see Table 5).

Other studies with the same kind of turboshaft engines and SAF show a similar behavior, where primarily aldehyde emissions were significantly influenced by the properties (paraffinic vs. aromatic) of the fuels (Cain et al. 2013). In Klingshirn et al. (2012) a helicopter engine with alternative fuels provided substantial reductions in UHC emissions in GI. This behavior could not be observed in the measurements carried out in this study. Spicer et al. (1984) reported that UHC are mainly composed of $\text{C}_{10}\text{--C}_{16}$ paraffins. More recent studies reported that emitted UHC are composed of small $\text{C}_2\text{--C}_6$ species and that high volatile and reactive $\text{C}_2\text{--C}_3$ alkenes dominate aircraft exhaust (Schürmann et al. 2007). The results of the APEX study partially confirmed previous data indicating that, in general, gaseous hydrocarbon emissions of various engines primarily consist of formaldehyde, ethylene, acetaldehyde, acetylene, propene, and others, while 16–42% of total non-methane hydrocarbons (NMHC) remained unresolved (Wey et al. 2006; Masiol and Harrison 2014).

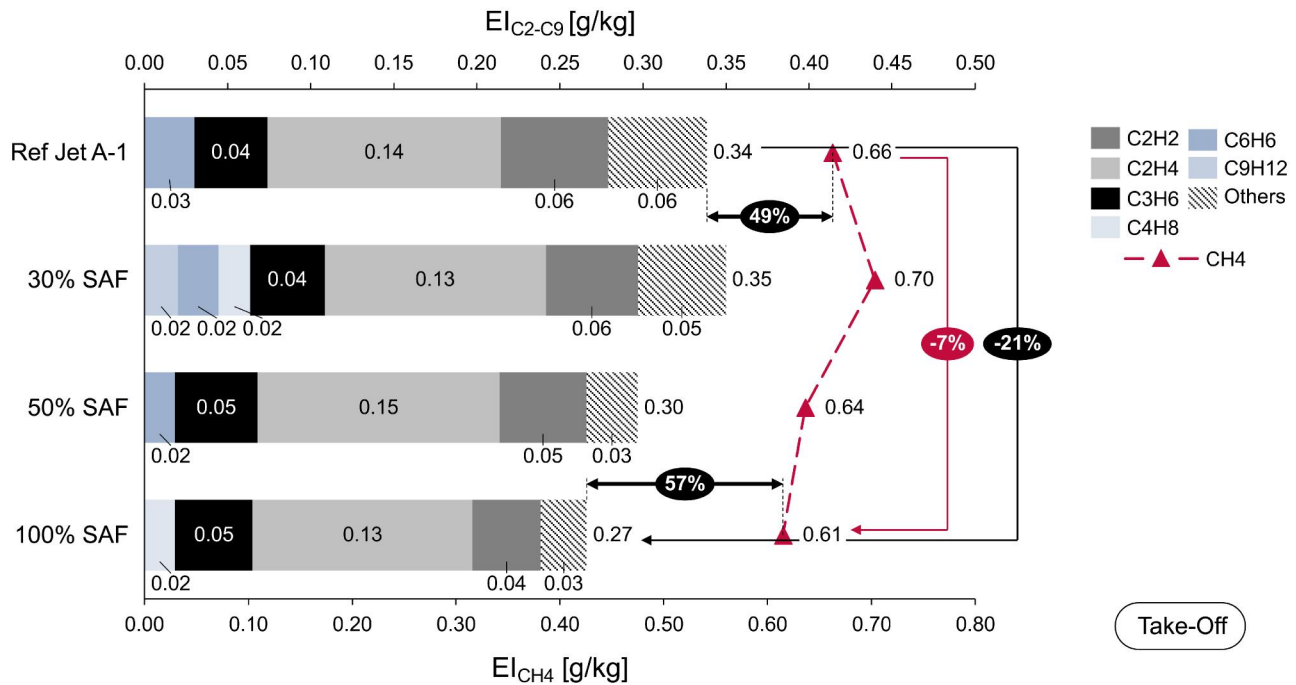


Figure 4. EI for methane (CH₄) and the ozone precursors C₂-C₉ for the engine power setting TO.

Table 5. EI [g/kg] for formaldehyde and acetaldehyde for TO and GI.

Compound		Ref Jet A-1	30% SAF	50% SAF	100% SAF
Take-Off					
Formaldehyde	CH ₂ O	0.08	0.09	0.09	0.07
Acetaldehyde	C ₂ H ₄ O	0.05	0.05	0.04	0.03
Ground-Idle					
Formaldehyde	CH ₂ O	3.24	3.46	3.61	4.13
Acetaldehyde	C ₂ H ₄ O	0.01	0.03	0.00	0.00

Non-volatile particulate matter emissions

Non-volatile particle number concentrations

EI_{numEP10} [# /kg] for all engine power settings are illustrated in Figure 5. The uncorrected averaged nvPM number concentrations [# /cm³] measured with the CPC are summarized in Table 6.

Figure 5 and Table 6 show that the number concentrations vary with engine power settings and with fuels used. Between TO and GI, 56% fewer particles per kilo of burnt fuel are emitted with Ref Jet A-1. The uncorrected number concentrations are comparable with measurements carried out on the same engine (Rohkamp et al. 2024). The highest uncorrected particle number concentration values are found at power setting LL with Ref Jet A-1 (see Table 6). Theoretically, the particle number concentrations should lower significantly between the power settings, as UHC are reduced by 98% (see Figure 2a) from “standard gaseous compounds” section and, at the same time, PAH should decrease in the same range as the combustion conditions are more complete. The reduction effect is more

evident as the proportion of SAF increases (shown in Figure 5 as an increase in the H/C ratio). It is noticeable that even small proportions of SAF cause a reduction in EI_{numEP10}. When Ref Jet-A1 and 100% SAF are directly compared, EI_{numEP10} can be reduced by 81% for the turboshaft engine at GI. With 100% SAF, the differences between power levels (and the associated reduction in soot precursors) also becomes more clear - here the number concentrations between TO and GI differ by 45%. It is noticeable that the EI_{numEP10} in GI at 100% SAF shows a clearly different behavior than with the blends or Ref Jet A-1. Despite the loss correction, significantly fewer soot particles are present there. This can be explained primarily by the size of the emitted particles. As the soot particles become smaller with increasing SAF content, the particle geometric mean diameter (GMD) shifts and therefore the correction calculation according to SAE ARP 6481 (SAE 2019) is no longer accurate, as correction is only made up to particles of 10 nm. And since the mode is in this lower limit, the values must be viewed critically, as significantly more particles can occur there. In addition, assumptions were made (e.g., soot particle density = 1 g/cm³) to perform the correction to the EENEP, which can influence the correction and results.

A possible explanation for the load and fuel-dependent reduction effects could be linked to the injection, mixing and combustion behavior. The low fuel feed pressure at GI results in few but relatively large fuel droplets. Therefore, a long-lasting locally

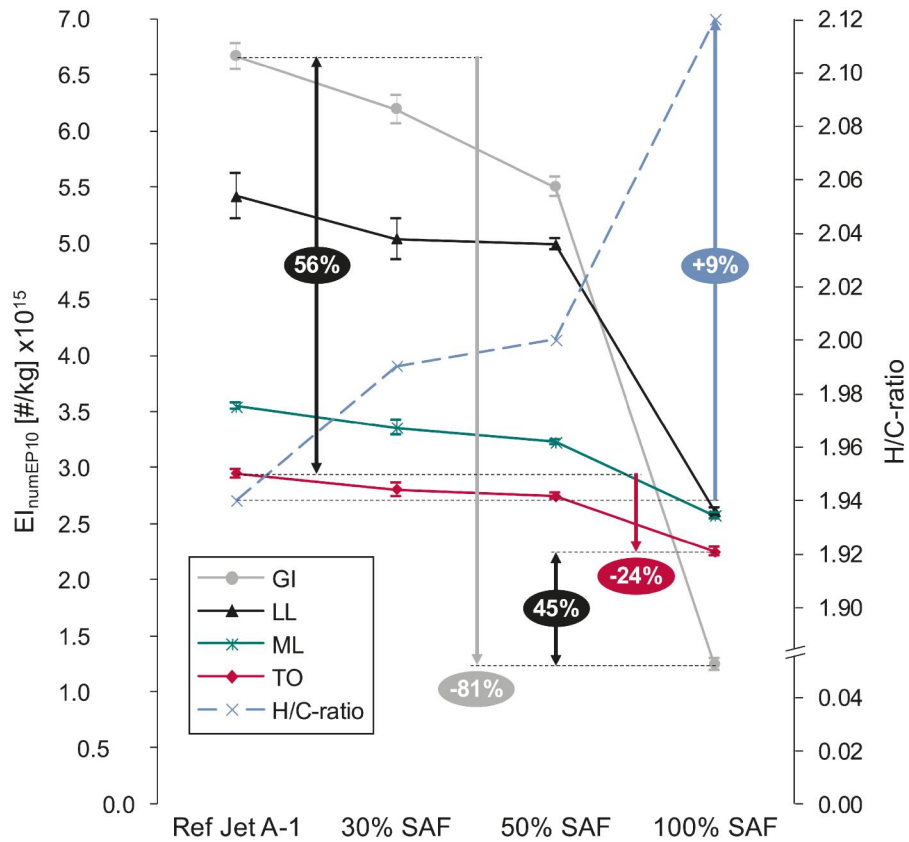


Figure 5. $EI_{numEP10}$ [#/#kg] plotted with the fuels used for all engine power settings.

Table 6. Averaged uncorrected nvPM number concentrations [#/#cm³] measured with CPC.

	Ref Jet-A1	30% SAF	50% SAF	100% SAF
GI	$4.22E+07 \pm 7.46E+05$	$3.59E+07 \pm 7.34E+05$	$3.01E+07 \pm 4.76E+05$	$7.53E+06 \pm 3.43E+05$
LL	$4.59E+07 \pm 1.72E+06$	$3.98E+07 \pm 1.42E+06$	$3.67E+07 \pm 3.76E+05$	$1.67E+07 \pm 2.36E+05$
ML	$4.42E+07 \pm 3.00E+05$	$3.91E+07 \pm 7.76E+05$	$3.70E+07 \pm 2.76E+05$	$2.42E+07 \pm 2.33E+05$
TO	$3.94E+07 \pm 5.16E+05$	$3.56E+07 \pm 7.82E+05$	$3.27E+07 \pm 3.45E+05$	$2.25E+07 \pm 3.49E+05$

rich combustion zone forms around these droplets. However, the flame is cooled down rapidly due to a high proportion of cooling air. It is assumed that PAHs form in the primary zone as a consequence of the high proportion of UHC and the presence of acetylene (Bockhorn 1994; C.K. Law 2006; Lieuwen and Yang 2013). With that, rapid ring formation is not supported by low temperatures (GI approx. 900 K) and particle growth (PAH nucleation) could be slowed down, which could lead to more but smaller soot particles or smaller PAH nuclei.

At TO, higher fuel feed pressure causes, comparable to GI, smaller but significantly more fuel droplets. The result is a better fuel atomization, faster vaporization and more homogeneous combustion. Higher temperatures (approx. 1200 K at the end of the combustor) are reached at this power setting. It can be assumed that the fuel in the primary zone can be

converted more efficiently. Less UHC are produced due to the higher heat release of the fuel-rich primary zone, and therefore, it is likely that, fewer but more long-chained PAHs are formed by faster reactions. Fewer particles are emitted at TO than in the other power settings for Ref Jet A-1. Adding SAF reverses the behavior so that fewer particles are emitted at GI than at LL, ML and TO. This behavior cannot be explained by the acetylene content in the exhaust gas, as more acetylene is formed at GI with 100% SAF (see Figure 3). This also cannot be explained by the emission species already listed but must be related to the composition of the fuel. It can be assumed that the reduction in $EI_{numEP10}$ is significantly more pronounced at GI than at TO as a result of fuel atomization (number of nuclei formed), more inefficient combustion with more UHC and due to the temperature-dependent formation of PAHs.

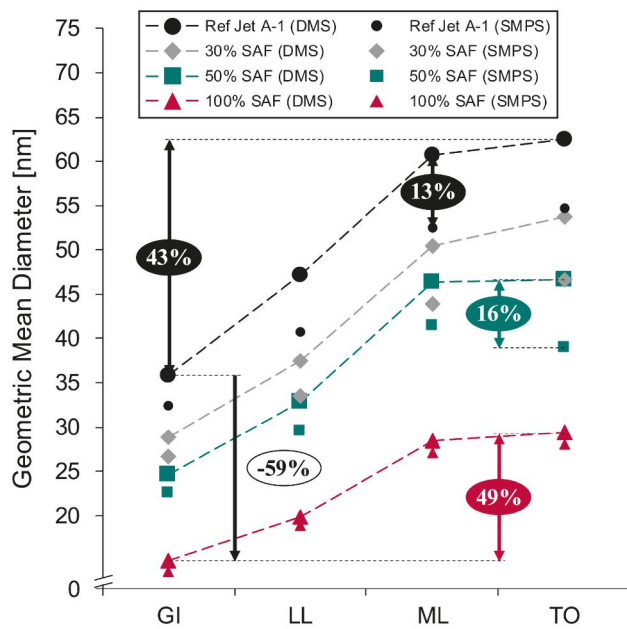


Figure 6. GMD [nm] of the PNSD measured with DMS500 and SMPS.

Non-volatile particle number size distributions and GMD

Figure 6 illustrates the GMD of the respective particle number size distributions (PNSD) for all engine power settings and fuels measured with DMS500 and SMPS. The different aerosol classification, quantification, aerosol charging and calibration of both instruments results in slightly varying values for the GMD. Deviations of up to 16% could be seen, however, the overall trend is the same: firstly, GMD increase with higher turboshaft engine power and, secondly, particle diameters become smaller as the SAF proportion increases. Furthermore, Figure 7 shows the different PNSD measured with SMPS. The graph clearly demonstrates the reduction in number of particles (area below the size distribution) and the dependence of the particle diameter on the engine power setting.

Power-Setting dependent GMD changes. Figure 6 shows that GMD measured with DMS500 changes from 62 nm (TO) to 35 nm (GI) for Ref Jet-A1. In comparison, for 100% SAF, the GMD is 29 nm for TO and 15 nm for GI. Basically, smaller soot particles form at lower power settings of the engine. This could be, among other things, due to lower number of soot particles inside the combustion chamber as less fuel is injected (comparison Table 1: 7.5 g/s vs. 24.0 g/s). This reduces the probability of coagulation of soot particles (Hinds and Zhu 2022). In addition, it can be assumed that rapid cooling of the exhaust gases could stop soot (or PAH) nucleation at an early stage so that smaller

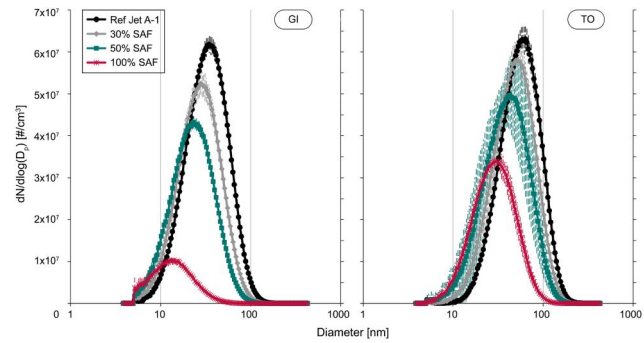


Figure 7. PNSD from all investigated fuels measured with SMPS.

particles are formed. The change of GMD related to the power-setting is characteristic for gas turbine engines and has also been demonstrated in modern thrust engines (with lean-burn combustion) (e.g., Lobo et al. 2015; Schripp et al. 2022; Durdina et al. 2024).

Fuel dependent GMD changes. The reduction in soot particle diameter may be attributed to higher hydrogen levels and/or lower aromatic contents in the fuel. This can be deduced as less PAH are formed when less carbon is available.

It can be summarized that, with the turboshaft engine used (and the associated fuel-rich primary combustion zone), the use of SAF has an influence on the size and number of nvPM formed. This had also been demonstrated in Kinsey et al. (2019). Soot reduction effects are not as significant as with LDI combustors (Lieuwen and Yang 2013; Corbin et al. 2022; Schripp et al. 2022), which could be a result of lower FAR and fewer PAH formation zones.

PM mass

Figures 8a and b illustrate the EI_{massEP10} of the fuels used for the engine power settings TO and GI for gravimetric filter sampling and for all engine power settings for the calculated SMPS PM mass. Both calculated EI show a PM mass decreases with increasing SAF content. The reduction in mass is the consequence of the reduction in GMD and the number of soot particles, as explained in “Non-volatile particulate matter emissions” section. The error bars are the largest for the Ref Jet A-1 fuel and the 30% blend for filter sampling. Deviations at TO are generally larger than at GI. The reduction behavior in EI_{numEP10} at GI with 100% SAF compared to Ref A-1 (81%, see Figure 5) can be recognized here as well. The soot mass was reduced in the same order of magnitude for TO (88% for SMPS mass and 76% for filter mass).

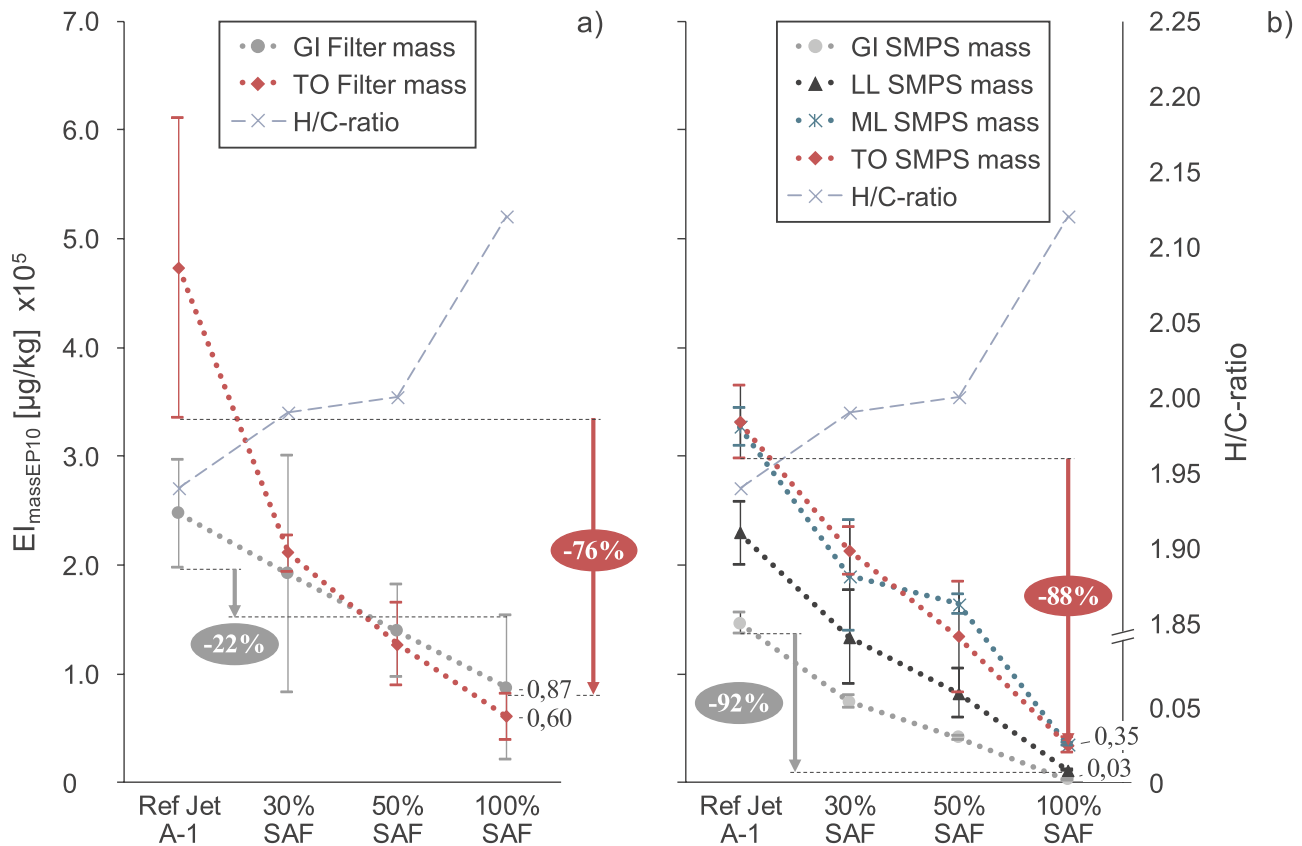


Figure 8. EI_{massEP10} [$\mu\text{g}/\text{kg}$] calculated with gravimetric filter mass and SMPS PNSD.

However, if the mass at GI engine power setting is compared, it is noticeable that the values differ significantly. For gravimetric filter sampling, the EI_{massEP10} is reduced by up to 22%, whereas the SMPS mass is reduced by 92%. This can be explained, among other things, by measurement inaccuracies (weighing, sample volume) and due to low particle masses caused by high dilution. For more details, see S4 of the [Supporting Information](#). The comparison of the two measuring principles shows that significantly more soot was detected with the filter sampling. Both techniques can be used for evaluation of PM mass, but it must be made clear that this can result in higher inaccuracies and both measurements do not meet the specifications made in the ICAO on PM mass measurements (ICAO 2023).

Summary and conclusions

A detailed emission characterization of a turboshaft engine (Allison 250-C20B) using alternative fuels (HEFA-SPK) was presented in this study. Two sustainable aviation fuel (SAF) blends (30%, 50%) as well as pure SAF and, as a reference, the blended Jet A-1 were used. The engine and especially the combustor

design results in a characteristic power-setting-dependent emission behavior. It was found out that the gaseous emissions (UHC, CO, and NO_x) regulated by ICAO have a negligible influence on emission indices (EI) when using SAF. However, a closer look at the gas phase and the UHC reveals that the volatile $\text{C}_2\text{--C}_9$ compounds, known as ozone precursors, behave differently. When using SAF, more volatile organic compounds (VOC) are emitted at low engine power settings. This trend is reversed for higher engine power settings, so that fewer VOC are emitted compared to the total UHC value and as a percentage with increasing SAF content. As a consequence of the chemical composition (almost no aromatics, no sulfur, and higher H/C ratio), SAF has, compared to Jet A-1, a lower tendency to form PAH in the used fuel-rich primary zone combustor. This underlines the results of the non-volatile particulate matter (nvPM) emissions. Soot particles arise from the gas phase compounds, explicitly through the formation of larger PAH. Changes in the number and mass concentrations of nvPM are much more significant than changes of gas phase constituents. At Ground-Idle, 100% SAF reduces the EI of nvPM number by more than 81% compared to regular Jet A-1. For Take-Off,

the reduction potential is 24%. An almost identical behavior can be seen for the EI of nvPM mass – here, 88% less mass is emitted by the engine at TO and almost 92% less mass at GI. The reduction in mass can be attributed to the shift in the size distributions, in particular, to the reduction in diameter (GMD). The soot particle diameters decrease almost linearly with the rising proportion of SAF for the engine used. However, the reduction potential must be viewed critically, as although a loss correction has been carried out, which only includes particles up to 10 nm. However, as soot particles with diameters smaller than 10 nm occur more frequently when using SAF, the number and mass concentrations can be significantly higher at the engine exit. The results of the gas turbine studies show that the use of SAF has great potential for reducing non-CO₂, in detail nvPM, emissions.

Nomenclature

AAFEX	Alternative aviation fuel experiment
APEX	Aircraft particle experiment
CO	Carbon monoxide
CO ₂	Carbon dioxide
CPC	Condensation particle counter
CS	Catalytic stripper
D _p	Particle diameter [nm]
DMA	Differential mobility analyzer
DMS	Differential mobility spectrometer
DL	Detection limit
EI	Emission index/emission indices [g/kg or mg/kg or #/kg]
EENEP	Engine exhaust nozzle exit plane
FAR	Fuel-air-ratio
ICAO	International Civil Aviation Organization
FID	Flame ionization detector
FOCA	Federal office of civil aviation
FOI	Swedish Defence Research Agency
FTIR	Fourier-transform-infrared
GC	Gas chromatograph
GMD	Geometric mean diameter [nm]
H/C-ratio	Hydrogen to carbon ratio
HEFA	Hydroprocessed esters and fatty acids
ICAO	International civil aviation organization
LB	Lean-burn
LPP	Lean-premixed-prevaporized
LTO	Landing-take-off
MW	Molar weight
NMHC	Non-methane hydrocarbons
NO _x	Nitric oxides
nvPM	Non-volatile particulate matter
PAH	Polycyclic aromatic hydrocarbons
PM	Particulate matter
PNSD	Particle number size distribution
PSD	Particle size distribution
RQL	Rich-burn quick-quench lean-burn
SAE	Society of automotive engineers
SAF	Sustainable aviation fuels
SMPS	Scanning mobility particle sizer

SPK	Synthetic paraffinic kerosene
STP	Standard temperature and pressure
TMB	Trimethylbenzene
UHC	Unburned hydrocarbons
VOC	Volatile organic compounds

Acknowledgements

We want to take this opportunity to thank Jesse Vilja and Reetu Sallinen (Neste) for providing the fuel and Lisa Ernle for supporting with VOC-GC measurements.



Disclosure statement

No potential conflict of interest was reported by the author(s).

Funding

The authors thank Munich Aerospace e. V. – Bavarian Research Alliance and the UniBw FORscience-project funding. In addition, this research [project LUKAS and MORE] is funded by dtec.bw – Digitalization and Technology Research Center of the Bundeswehr. Dtec.bw is funded by the European Union – NextGenerationEU. This research was also supported by the project ULTRHAS– Ultrafine particles from TRansportation – Health Assessment of Sources, a project funded under the EU’s Research and Innovation programme Horizon 2020, Grant Agreement No. 955390. Furthermore, we acknowledge financial support for open access publication by University of the Bundeswehr Munich.

ORCID

Marius Rohkamp  <http://orcid.org/0009-0003-4112-2864>
 Jan Bendl  <http://orcid.org/0000-0003-2322-5483>
 Thomas Adam  <http://orcid.org/0009-0005-3449-1885>

References

- Adam, T. W., C. Astorga, M. Clairotte, M. Duane, M. Elsasser, A. Krasenbrink, B. R. Larsen, U. Manfredi, G. Martini, L. Montero, et al. 2011. Chemical analysis and ozone formation potential of exhaust from dual-fuel (liquefied petroleum gas/gasoline) light duty vehicles. *Atmos. Environ.* 45(17):2842–8. doi: [10.1016/j.atmosenv.2011.03.002](https://doi.org/10.1016/j.atmosenv.2011.03.002).
- Anderson, B. E., A. J. Beyersdorf, C. H. Hudgins, J. V. Plant, K. L. Thornhill, E. L. Winstead, L. D. Ziemba, R. Howard, E. Corporan, R. C. Miake-Lye, et al. 2011. Alternative aviation fuel experiment (AAFEX). Tech. Rep. NASA/TM-2011-217059, NASA.
- Bockhorn, H. 1994. *Soot formation in combustion: Mechanisms and models*. Berlin: Springer. doi: [10.1007/978-3-642-85167-4](https://doi.org/10.1007/978-3-642-85167-4).
- Boies, A. M., M. E. J. Stettler, J. J. Swanson, T. J. Johnson, J. S. Olfert, M. Johnson, M. L. Eggersdorfer, T. Rindlisbacher, J. Wang, K. Thomson, et al. 2015. Particle

- emission characteristics of a gas turbine with a double annular combustor. *Aerosol Sci. Technol.* 49 (9):842–55. doi: [10.1080/02786826.2015.1078452](https://doi.org/10.1080/02786826.2015.1078452).
- Brem, B. T., L. Durdina, F. Siegerist, P. Beyerle, K. Bruderer, T. Rindlisbacher, S. Rocci-Denis, M. G. Andac, J. Zelina, O. Penanhoat, et al. 2015. Effects of fuel aromatic content on nonvolatile particulate emissions of an in-production aircraft gas turbine. *Environ. Sci. Technol.* 49 (22):13149–57. doi: [10.1021/acs.est.5b04167](https://doi.org/10.1021/acs.est.5b04167).
- Cain, J., M. J. DeWitt, D. Blunck, E. Corporan, R. Striebich, D. Anneken, C. Klingshirn, W. M. Roquemore, and R. Vander Wal. 2013. Characterization of gaseous and particulate emissions from a turboshaft engine burning conventional, alternative, and surrogate fuels. *Energy Fuels* 27 (4):2290–302. doi: [10.1021/ef400009c](https://doi.org/10.1021/ef400009c).
- Corbin, J. C., T. Schripp, B. E. Anderson, G. J. Smallwood, P. LeClercq, E. C. Crosbie, S. Achterberg, P. D. Whitefield, R. C. Miake-Lye, Z. Yu, et al. 2022. Aircraft-engine particulate matter emissions from conventional and sustainable aviation fuel combustion: Comparison of measurement techniques for mass, number, and size. *Atmos. Meas. Tech.* 15 (10):3223–42. doi: [10.5194/amt-15-3223-2022](https://doi.org/10.5194/amt-15-3223-2022).
- Drozd, G. T., M. A. Miracolo, A. A. Presto, E. M. Lipsky, D. D. Riemer, E. Corporan, and A. L. Robinson. 2012. Particulate matter and organic vapor emissions from a helicopter engine operating on petroleum and Fischer-Tropsch Fuels. *Energy Fuels* 26 (8):4756–66. doi: [10.1021/ef300651t](https://doi.org/10.1021/ef300651t).
- Durand, E., L. Durdina, G. Smallwood, M. Johnson, C. Spirig, J. Edebeli, M. Roth, B. Brem, Y. Sevcenco, and A. Crayford. 2023. Correction for particle loss in a regulatory aviation nvPM emissions system using measured particle size. *J. Aerosol Sci.* 169:106140. doi: [10.1016/j.jaerosci.2023.106140](https://doi.org/10.1016/j.jaerosci.2023.106140).
- Durand, E., P. Lobo, A. Crayford, Y. Sevcenco, and S. Christie. 2021. Impact of fuel hydrogen content on non-volatile particulate matter emitted from an aircraft auxiliary power unit measured with standardised reference systems. *Sci. Technol. Fuel Energy* 287:119637. doi: [10.1016/j.fuel.2020.119637](https://doi.org/10.1016/j.fuel.2020.119637).
- Durdina, L., B. T. Brem, M. Elser, D. Schönenberger, F. Siegerist, and J. G. Anet. 2021. Reduction of nonvolatile particulate matter emissions of a commercial turbofan engine at the ground level from the use of a sustainable aviation fuel blend. *Environ. Sci. Technol.* 55 (21):14576–85. doi: [10.1021/acs.est.1c04744](https://doi.org/10.1021/acs.est.1c04744).
- Durdina, L., E. Durand, J. Edebeli, C. Spirig, B. T. Brem, M. Elser, F. Siegerist, M. Johnson, Y. A. Sevcenco, and A. P. Crayford. 2024. Characterizing and predicting nvPM size distributions for aviation emission inventories and environmental impact. *Environ. Sci. Technol.* 58 (24):10548–57. doi: [10.1021/acs.est.4c02538](https://doi.org/10.1021/acs.est.4c02538).
- EU Directive 2008. European Union Directive 2008/50/EC of the European Parliament and of the Council of 21 May 2008 on ambient air quality and cleaner air for Europe. Accessed November 26, 2023. <https://eur-lex.europa.eu/legal-content/en/TXT/?uri=CELEX%3A32008L0050>
- Harper, J., E. Durand, P. Bowen, D. Pugh, M. Johnson, and A. Crayford. 2022. Influence of alternative fuel properties and combustor operating conditions on the nvPM and gaseous emissions produced by small-scale RQL combustor. *Sci. Technol. Fuel Energy* 315:123045. doi: [10.1016/j.fuel.2021.123045](https://doi.org/10.1016/j.fuel.2021.123045).
- Hicks, Y. R., and K. M. Tacina. 2021. Design Guidelines for Swirl-Venturi Fuel-Air Mixers for Lean Direct Injection Combustors. NASA/TM-20210011787. Glenn Research Center, Cleveland, Ohio.
- Hinds, W. C., and Y. Zhu. 2022. *Aerosol technology – properties, behavior, and measurement of airborne particles*. New York: John Wiley & Sons Inc.
- Hupfer, A. 2007. *Kraftstoffeinspritzsysteme für Vormischbrenner kleiner Fluggasturbinen [Fuel injection systems for premix burners of small aircraft gas turbines]*. München: Verlag Dr. Hut.
- International Civil Aviation Organization (ICAO). 2023. *Annex 16 to the Convention of International Civil Aviation Organization: Environmental protection: Volume II - Aircraft Engine Emissions*. 4th ed. Montreal, Quebec, Canada: International Standards and Recommended Practices. <https://www.bazl.admin.ch/bazl/en/home/themen/legislation/anhaenge-icao.html>.
- Kinsey, J. S., E. Corporan, J. Pavlovic, M. DeWitt, C. Klingshirn, and R. Logan. 2019. Comparison of measurement methods for the characterization of the black carbon emissions from a T63 turboshaft engine burning conventional and Fischer-Tropsch fuels. *J. Air Waste Manag. Assoc.* 69 (5):576–91. doi: [10.1080/10962247.2018.1556188](https://doi.org/10.1080/10962247.2018.1556188).
- Klingshirn, C. D., M. DeWitt, R. Striebich, D. Anneken, L. Shafer, E. Corporan, M. Wagner, and D. Brigalli. 2012. Hydroprocessed renewable jet fuel evaluation, performance, and emissions in a T63 turbine engine. *ASME. J. Eng. Gas Turbines Power* 134 (5):051506. doi: [10.1115/1.4004841](https://doi.org/10.1115/1.4004841).
- Kulkarni, P., P. A. Baron, and K. Willeke. 2011. *Aerosol measurement: Principles, techniques, and applications*. 3rd ed. Hoboken: John Wiley & Sons Inc. doi: [10.1002/9781118001684](https://doi.org/10.1002/9781118001684).
- Law, C. K. 2006. *Combustion physics*. Cambridge: Cambridge University Press. doi: [10.1017/CBO9780511754517](https://doi.org/10.1017/CBO9780511754517).
- Lee, D. S., D. W. Fahey, A. Skowron, M. R. Allen, U. Burkhardt, Q. Chen, S. J. Doherty, S. Freeman, P. M. Forster, J. Fuglestedt, et al. 2021. The contribution of global aviation to anthropogenic climate forcing for 2000 to 2018. *Atmos. Environ. (1994)* 244:117834. doi: [10.1016/j.atmosenv.2020.117834](https://doi.org/10.1016/j.atmosenv.2020.117834).
- Lefebvre, A. H., and D. R. Ballal. 2010. *Gas turbine combustion – alternative fuels and emissions*. 3rd ed. Boca Raton, Florida: CRC Press Taylor & Francis Group.
- Lieuwen, T. C., and V. Yang. 2013. *Gas turbine emissions*. New York, USA: Cambridge University Press.
- Lobo, P., L. Durdina, G. J. Smallwood, T. Rindlisbacher, F. Siegerist, E. A. Black, Z. Yu, A. A. Mensah, D. E. Hagen, R. C. Miake-Lye, et al. 2015. Measurement of aircraft engine non-volatile PM emissions: Results of the aviation-particle regulatory instrumentation demonstration experiment (A-PRIDE) 4 Campaign. *Aerosol Sci. Technol.* 49 (7):472–84. doi: [10.1080/02786826.2015.1047012](https://doi.org/10.1080/02786826.2015.1047012).
- Masiol, M., and R. M. Harrison. 2014. Aircraft engine exhaust emissions and other airport-related contributions to ambient air pollution: A review. *Atmos. Environ. (1994)* 95:409–55. doi: [10.1016/j.atmosenv.2014.05.070](https://doi.org/10.1016/j.atmosenv.2014.05.070).

- Moore, R. H., M. Shook, A. Beyersdorf, C. Corr, S. Herndon, W. B. Knighton, R. Miake-Lye, K. L. Thornhill, E. L. Winstead, Z. Yu, et al. 2015. Influence of jet fuel composition on aircraft engine emissions: A synthesis of aerosol emissions data from the NASA APEX, AAFEX, and ACCESS missions. *Energy Fuels* 29 (4):2591–600. doi: [10.1021/ef502618w](https://doi.org/10.1021/ef502618w).
- Moore, R. H., K. L. Thornhill, B. Weinzierl, D. Sauer, E. D'Ascoli, J. Kim, M. Lichtenstern, M. Scheibe, B. Beaton, A. J. Beyersdorf, et al. 2017. Biofuel blending reduces particle emissions from aircraft engines at cruise conditions. *Nature* 543 (7645):411–5. doi: [10.1038/nature21420](https://doi.org/10.1038/nature21420).
- Owen, B., J. G. Anet, N. Bertier, S. Christie, M. Cremaschi, S. Dellaert, J. Edebeli, U. Janicke, J. Kuenen, L. Lim, et al. 2022. Review: Particulate matter emissions from aircraft. *Atmosphere* 13 (8):1230. doi: [10.3390/atmos13081230](https://doi.org/10.3390/atmos13081230).
- Rindlisbacher, T., and L. Chabbey. 2015. Guidance on the Determination of Helicopter Emissions. Report number: COO.2207.111.2.2015750, Swiss Confederation, Bern, Swiss.
- Rohkamp, M., A. Rabl, B. Gündling, M. R. Saraji-Bozorgzad, C. Mull, J. Bendl, C. Neukirchen, C. Helcig, T. Adam, V. Gümmer, et al. 2024. Detailed gaseous and particulate emissions of an Allison 250-C20B turboshaft engine. *J. Eng. Gas Turbines Power* 146 (4):041009. doi: [10.1115/1.4063693](https://doi.org/10.1115/1.4063693).
- Schripp, T., B. E. Anderson, U. Bauder, B. Rauch, J. C. Corbin, G. J. Smallwood, P. Lobo, E. C. Crosbie, M. A. Shook, R. C. Miake-Lye, et al. 2022. Aircraft engine particulate matter emissions from sustainable aviation fuels: Results from ground-based measurements during the NASA/DLR campaign ECLIF2/ND-MAX. *Fuel* 325: 124764. doi: [10.1016/j.fuel.2022.124764](https://doi.org/10.1016/j.fuel.2022.124764).
- Schürmann, G., K. Schäfer, C. Jahn, H. Hoffmann, M. Bauerfeind, E. Fleuti, and B. Rappenglück. 2007. The impact of NO_x, CO and VOC emissions on the air quality of Zurich airport. *Atmos. Environ.* 41 (26):103–18.
- Society of Automotive Engineers International (SAE 2016) 2016. *SAE Aerospace Recommended Practice (ARP) 1533 C - Procedure for the analysis and evaluation of gaseous emissions from aircraft engines*. 4th ed. Warrendale, PA: SAE International.
- Society of Automotive Engineers International (SAE 2019) 2019. *SAE Aerospace Recommended Practice (ARP) 6481 - Procedure for the calculation of non-volatile particulate matter sampling and measurement system losses and system loss correction factors*. 1st ed. Warrendale, PA: SAE International.
- Society of Automotive Engineers International (SAE 2021) 2021. *SAE Aerospace Recommended Practice (ARP) 6320 A - Procedure for the continuous sampling and measurement of non-volatile particulate matter emissions from aircraft turbine engines*. 2nd ed. Warrendale, PA: SAE International.
- Society of Automotive Engineers International (SAE 2022) 2022. *SAE Aerospace Information Report (AIR) 6504 - Procedure for the Calculation of non-volatile Particulate Matter Sampling and Measurement System Penetration Functions and System Loss Correction Factors*. 1st ed. Warrendale, PA: SAE International.
- Spicer, C. W., M. W. Holdren, T. F. Lyon, and R. M. Rigglin. 1984. Composition and Photochemical Reactivity of Turbine Engine Exhaust. Report No. AD-A150 559. Air Force Engineering and Services Center. Tyndall AFB, Florida.
- Voigt, C., J. Kleine, D. Sauer, R. H. Moore, T. Bräuer, P. Le Clercq, S. Kaufmann, M. Scheibe, T. Jurkat-Witschas, M. Aigner, et al. 2021. Cleaner burning aviation fuels can reduce contrail cloudiness. *Commun. Earth Environ.* 2 (1):114. doi: [10.1038/s43247-021-00174-y](https://doi.org/10.1038/s43247-021-00174-y).
- Wey, C. C., B. E. Anderson, C. Hudgins, C. Wey, X. Li-Jones, E. Winstead, L. K. Thornhill, P. Lobo, D. Hagen, P. Whitefield, et al. 2006. Aircraft Particle Emissions eXperiment (APEX). Report Number: E-15660. National Aeronautics and Space Administration. Cleveland, Ohio.